RSC Advances

ROYAL SOCIETY OF CHEMISTRY

www.rsc.org/advances

Ultradrawing Properties of Ultrahigh Molecular Weight Polyethylenes / Functionalized Activated Nanocarbon As-prepared Fibers

Wang-xi Fan[a,b], Chuen-kai Wang[c], Chih-chen Tsai[c], Yi Ding[a], Zhong-dan Tu[a], Chao-Ming Huang[d], Kuo-Shien Huang[c] and Jen-taut Yeh[*a, c, d]

[*a] Hubei Collaborative Innovation Center for Advanced Organic Chemical Materials Ministry of Education, Key Laboratory for the Green Preparation and Application of Functional Materials, Faculty of Materials Science and Engineering, Hubei University, Wuhan, China

E-mail: jyeh@mail.ntust.edu.tw

[b] Department of Chemical and Environmental Engineering, Wuhan Bioengineering Institute, Wuhan, China

[c] Graduate School of Material Science and Engineering National Taiwan University of Science and Technology, Taipei, Taiwan

[d] Department of Materials Engineering, Kun Shan University, Tainan, Taiwan

Abstract

The improvement of the ultradrawing and ultimate tensile properties of high performance fibers is the most critical and challenging one for the applications of high

performance fibers, such as ultra high molecular weight polyethylene (UHMWPE) fibers. This paper aims to improve the ultradrawing and ultimate tensile properties of UHMWPE fibers by incorporating very small amounts of nanofillers during gel spinning process of UHMWPE fibers. Activated nanocarbon (ANC), acid treated activated nanocarbon (ATANC) and functionalized activated nanocarbon (FANC) prepared by grafting maleic anhydride polyethylene onto ATANC, were added into the UHMWPE fibers as effective nucleation nanofillers with specific surface areas higher than 1000 m^2g^{-1}. It is the first work that ANC, ATANC and FANC were used as reinforced or functional additives in UHMWPE composite fibers to enhance their ultradrawing and/or ultimate tensile properties. The experimental results show that the maximum achievable draw ratio obtained for the best prepared UHMWPE/FANC fiber reaches 398 and the ultimate tensile strength (σ_f) of the best prepared UHMWPE/FANC drawn fiber reaches around 7.8 GPa, when the mass fraction of FANC is 0.075 phr. They are the highest draw ratios and σ_f values obtained so far for UHMWPE/nanofiller composite fibers reported in the literatures.

Key words: ultradrawing, activated nanocarbon, specific surface areas, ultrahigh molecular weight polyethylene.

Introduction

High performance fibers, such as ultrahigh molecular weight polyethylene (UHMWPE) fibers have attracted lots of attention and have become one of the research hotspots owing to its good properties, such as, low density, excellent tenacity, flexibility, bio-compatibility properties, ultraviolet and chemical stability since the 1980s. They have been extensively used for various application areas, such as, bulletproof vests, safety textiles, luggage weaving, marine ropes and high strength composite materials. Ultra high molecular weight polyethylene[1-39], Polypropylene[40-41] and Poly(vinyl alcohol)[42-43] fibers are typical high performance fibers produced using the gel spinning processing method from flexible polymer chains. The key element in obtaining high-strength UHMWPE fibers is to find a way to draw the as-prepared gel specimens to an ultrahigh draw ratio after the gel spinning process. The drawability of the as-prepared gel fibers was found to depend significantly on the compositions of gel solutions[6-14], cooling temperatures used in the air atmosphere after gel spinning[2, 10, 16, 21, 24-30] and drawing conditions used after preparation of the as-prepared fibers[4, 9-10, 15, 19-22].

Our recent investigations[31-38] found that inorganic or organic nanofillers with extremely high specific surface areas can act as efficient nucleation sites and significantly improve the achievable draw ratios and ultimate tenacity properties of nanofillers filled UHMWPE fibers. In which, nanofillers (*e.g.* carbon nanotube[31-35], attapulgite[36], nanosilica, modified nanosilica[37] and modified bacterial cellulose nanofillers[38]) with extremely high specific surface areas ($\geqq$ 150 m^2g^{-1}) can serve as efficient nucleation sites and facilitate the crystallization of UHMWPE molecules into crystals but with lower melting temperatures and/or evaluated smaller crystal thickness values during their crystallization processes. In fact, the ultimate tensile strength values of the UHMWPE/purified attapulgite, UHMWPE/functionalized carbon nanotube, UHMWPE/functionalized

nanosilica and UHMWPE/modified bacterial cellulose drawn fibers prepared using one-stage drawing process at 95 ℃ can reach 4.7, 5.8, 7.0 and 7.1 GPa, respectively, which is about 1.74, 2.15, 2.59 and 2.63 times of that of the corresponding UHMWPE drawn fibers prepared at the same optimal UHMWPE concentration, cooling and drawing condition but without incorporation of any modified nanofiller.

In contrast to carbon nanotubes, bacterial cellulose nanofibers or nanosilica particles, activated nanocarbons (ANC) are commercially available nanoparticles with even higher specific surface areas than those nanoparticles used in our previous investigations[31-38]. Some commercially available ANC particles are reported to have specific surface areas higher than 1000 m^2g^{-1},[44] which are the highest specific surface areas commercially available in the market of nanoparticles. Owing to their well-developed internal surface and excellent electrical conductivity, activated nanocarbons are commonly used as adsorbent or electrode materials in numerous applications[45-49]. However, activated nanocarbons have never been used as reinforced or functional additives in UHMWPE composite fibers to enhance their ultradrawing and/or ultimate tensile properties. In this study, acid treated and functionalized activated nanocarbon (ATANC, FANC) particles were used as an efficient nucleation agent to improve the ultradrawing and ultimate tensile properties of UHMWPE/ATANC and UHMWPE/FANC fibers. The achievable draw ratios of UHMWPE/ATANC and UHMWPE/FANC as-prepared fibers approached a maximal value as their ATANC and FANC contents reached an optimal value, respectively. In which, the maximal achievable draw ratios obtained for UHMWPE/FANC as-prepared fiber specimens and ultimate tensile strength values of UHMWPE/FANC drawn fiber specimens are even higher than those of UHMWPE/purified attapulgite, UHMWPE/modified bacterial cellulose, UHMWPE/functionalized carbon nanotube and UHMWPE/functionalized nanosilica fiber

specimens prepared at their optimal nanofiller contents, respectively, in our previous investigations[31-38]. Specific surface area, morphological and Fourier transform infrared analyses of the ANC, ATANC and FANC particles and investigations on thermal, dynamic mechanical, orientation factor and ultimate tensile properties of the as-prepared and/or drawn UHMWPE/ATANC and UHMWPE/FANC fiber specimens were performed to understand the above improved ultradrawing and ultimate tensile properties of the UHMWPE/ATANC and UHMWPE/FANC as-prepared fiber specimens.

Experimental

Materials

The UHMWPE GUR-4120 resin used in this study is associated with a weight-average molecular weight (Mw) of 5.0×10^6, which was kindly supplied by Celanese (Nanjing) Diversified Chemical Corporation located in Nanjing, China. The activated nanocarbon (ANC) HN-60 used in this study were purchased from Shanghai Hainuo Charcoal Corporation from Shanghai, China. Approximate 1200 m^2g^{-1} was quoted as the specific surface area for ANC particles by Shanghai Hainuo Charcoal Corporation. Maleic anhydride grafted polyethylene ($PE_{g\text{-}MAH}$) resin was used to modify ATANC particles, where $PE_{g\text{-}MAH}$ resin was purchased from Langfang Plastic Corporation, Langfang, China.

Sample preparation

One-tenth gram of ANC was dispersed and modified in 100 ml of concentrated H_2SO_4/HNO_3 (1:3 v/v) solution at 140 ℃ for 40 minutes under stirring condition. The acid treated ANC (ATANC) particles were then dried in a vacuum oven at 100 ℃ for 12 hours. The functionalized ANC (FANC) particles were then prepared by grafting $PE_{g\text{-}MAH}$ molecules onto the ATANC particles in ultrasonicated mixtures of decalin, ATANC and $PE_{g\text{-}MAH}$ at 170 ℃ for 1 hour. The functionalized ANC particles prepared above will be referred to as $FANC^{mx}$ particles in the following discussion. In which, the superscript *x* denotes the weight ratio of $PE_{g\text{-}MAH}$ to ATANC used in the preparation processes of $FANC^{mx}$ particles. The sample designations of $FANC^{mx}$ and weight ratios of $PE_{g\text{-}MAH}$ to ATANC used in the functionalizing experiments of $FANC^{mx}$ particles are summarized in table 1.

Varying contents of ANC, ATANC and $FANC^{mx}$ particles together with UHMWPE

resin were dispersed and/or dissolved in decalin at 135 ℃ for 1.5 hours, respectively, in which 0.1% di-t-butyl-p-cresol was added as an antioxidant. The UHMWPE, UHMWPE/ANC, UHMWPE/ATANC and UHMWPE/FANC^{mx} gel solutions prepared above were then fed into a temperature-controlled hopper and kept as hot homogenized gel solutions before spinning. Detailed experimental procedures for preparation of UHMWPE (F_{100}), UHMWPE/ANC ($F_{100}ANC_y$), UHMWPE/ATANC ($F_{100}ATANC_y$), and UHMWPE/FANC^{mx} ($F_{100}FANC^{mx}_y$) as-prepared fibers were reported in our previous investigations[31-38]. In which, the subscript 100 denotes one hundred parts of UHMWPE resins used in the as-prepared fibers; the superscript *x* denotes the weight ratio of $PE_{g\text{-}MAH}$ to ATANC used in the preparation processes of FANC^{mx} particles; the subscript *y* denotes parts of ANC, ATANC, or FANC^{mx} particles used in per hundred parts of UHMWPE resins. Table 2 summarized designations of typical UHMWPE, UHMWPE/ANC and UHMWPE/ATANC and UHMWPE/FANC^{mx} as-prepared fiber specimens and the corresponding compositions of gel solutions used in the gel spinning processes.

Fourier transform infrared spectroscopy

Fourier transform infrared (FT-IR) spectroscopic measurements of the $PE_{g\text{-}MAH}$, ANC, ATANC and FANC^{mx} specimens were recorded on a Nicolet Avatar 360 FT-IR spectrophotometer at 25 ℃, wherein 32 scans with a spectral resolution 1 cm^{-1} were collected during each spectroscopic measurement. FT-IR analyses of the ANC, ATANC and FANC^{mx} particles were performed only to reveal the qualitative but not the exact amount of functional group anchored on the above particles. Infrared spectra of the $PE_{g\text{-}MAH}$, ANC, ATANC and FANC^{mx} film specimens were determined using the conventional KBr disk method. Decalin, alcohol, alcohol and decalin solutions containing $PE_{g\text{-}MAH}$, ANC, ATANC or FANC^{mx} particles, respectively, were cast onto KBr

disk and dried at 60 ℃ for 30 minutes. The cast films used in this study were prepared sufficiently thin enough to obey the Beer-Lambert law.

Morphological analysis

In order to observe the morphology on the surfaces of ANC, ATANC and FANC^{mx} particles prepared in the "Materials and Sample Preparation" section, the ANC and ATANC particles were dispersed in alcohol, while FANC^{mx} particles were dispersed in decalin to have a better dispersed morphology before examination. Before morphological analyses, ten micrograms of ANC, ATANC and FANC^{mx} particles were added and ultrasonicated in 10 ml alcohol, alcohol and decalin at 25 ℃ for 5 minutes, respectively. The dispersed particles were then dried onto a carbon-coated copper grid under ambient conditions prior to morphological analyses. The cast ANC, ATANC and FANC^{mx} particles were then examined using a Philip transmission electron microscope (TEM) model Tecnai G20 operated at 100 kV.

Specific surface area analysis

A Laser Particle Size Analyzer model BT-9300H (Dandong Bettersize Instruments Corporation, Dandong, China) was used to study the specific surface areas of the ANC, ATANC and FANC^{mx} particles. Before analyses, ten micrograms of ANC, ATANC and FANC^{mx} particles were added and ultrasonicated in 10 ml alcohol, alcohol and decalin at 25 ℃ for 5 minutes, respectively. The specific surface areas of ANC, ATANC and FANC^{mx} particles were then measured by placing the ultrasonicated solutions prepared above in the curette of the Laser Particle Size Analyzer at 25 ℃.

Thermal and orientation factor analysis

The thermal properties of as-prepared fiber specimens were performed on a Du Pont differential scanning calorimeter (DSC) model 2000. All scans were carried out at a heating rate of 20 ℃/min under flowing nitrogen at a flow rate of 25 ml/min. Samples weighing 0.5 mg and 15 mg were placed in the standard aluminum sample pans for determination of their melting temperature (T_m) and percentage crystallinity (X_c) values, respectively. The X_c values of the as-prepared fiber specimens were estimated using baselines drawn from 40 to 160℃ and a perfect heat of fusion of polyethylene of 293 J/g [50]. With the base line drawing from 60 to 160°C and 15 mg of testing specimens, the error in estimating X_c is around ±0.5%. In contrast, the error in determination of the melting temperatures of the as-prepared fiber specimens using 0.5 mg can be reduced to about ±0.1°C, since the effect of thermal lag resulted from thermal insulation of UHMWPE resins during the DSC heat scanning experiment is significantly reduced.

In order to understand the ultradrawing properties of UHMWPE, UHMWPE/ATANC and UHMWPE/FANC^{mx} as-prepared fiber specimens, the lamellar thickness (l_c) values of the above as-prepared fibers were evaluated from their T_m values using Hoffman and Week's equation[50, 51] given in *eq*. (1). In which, an equilibrium melting temperature (T_m^0) of 145.5 ℃, a perfect heat of fusion (ΔH_f^0) of 293 J·g^{-1} and a folded surface free energy (σ_e) of 9×10^{-6} J·cm^{-2} of polyethylene crystals[50] were used for evaluation of l_c values of UHMWPE, UHMWPE/ANC, UHMWPE/ATANC and UHMWPE/FANC^{mx} as-prepared fiber specimens.

$$T_m = T_m^o \left[1 - \frac{2\sigma_e}{l_c \Delta H_f^0}\right] \quad (1)$$

The orientation factor (f_o) values of UHMWPE, UHMWPE/ATANC and UHMWPE/FANC^{mx} as-prepared and drawn fiber specimens were measured using a sonic velocity orientation instrument model SCY-Ⅲ, which was purchased from Donghuakaili

Chemicals and Fiber Technology Corporation, Shanghai, China. Before testing, the fiber specimen with 60 cm in length was wound and clamped on a testing device with a span of 40 cm. The f_o values of the as-spun and drawn fiber specimens were then measured at 25 ℃. A minimum of five samples of each specimen were tested and averaged during the orientation measurements. The f_o values were evaluated using *eq*. (2) as suggested by Xiao and coauthors[52]:

$$f_s = 1 - (C_u / C)^2 \quad (2)$$

where C is the sonic velocity of the as-prepared or drawn UHMWPE fiber specimen and C_u is the sonic velocity of the fully unoriented sample, taken as 1.65 km/s[52].

Dynamic mechanical properties

A TA dynamic mechanical analysis (DMA) unit model Q800 was used to study the mechanical relaxation of the as-prepared fiber specimen. All DMA experiments were operated at a frequency of 1 Hz, a heating rate of 2 ℃/min and in a temperature range from -150 to 150 ℃.

Drawing and tensile properties of the fiber specimens

The UHMWPE, UHMWPE/ANC, UHMWPE/ATANC and UHMWPE/FANC^{mx} fiber specimens used in the drawing experiments were cut from the dried as-prepared fibers and then stretched on a Gotech tension testing machine model GT-TFS-2000 equipped with a temperature-controlled oven. The fibers are 20 mm in length, which were wound and clamped in a stretching device and then stretched at a crosshead speed of 20 mm/min and at a constant temperature of 95 ℃. The draw ratio of each fiber specimen was determined as the ratio of the marked displacement after and before drawing. The marked displacement before drawing was 27 mm. The tensile properties of the

as-prepared and drawn fibers were determined using a Hung-Ta tension testing machine model HT-9112 at a crosshead speed of 20 mm/min. A minimum of five samples of each specimen were tested and averaged during the tensile experiments.

Results and Discussion

Fourier transform infra-red spectroscopy

Fig. 1 illustrates typical Fourier transform infra-red (FT-IR) spectra of ANC, ATANC, FANC^{mx} and maleic anhydride grafted polyethylene ($PE_{g\text{-}MAH}$) specimens. As shown in Fig. 1a, three distinguished absorption bands centered at 1380, 1690 and 3443 cm^{-1} corresponding to the motions of methyl -CH_3 bending vibration, carboxylic C=O and -OH stretching vibrations[53-55], respectively, were found in the spectrum of the ANC specimen. The $PE_{g\text{-}MAH}$ specimen exhibited two distinctive absorption bands centered at 1710 and 1791 cm^{-1}, which were generally attributed to the motion of O-C=O and C=O stretching vibrations of maleic anhydride[6, 55] (see Fig. 1h). After etching by H_2SO_4/HNO_3 solutions (1:3 v/v) for 40 minutes, the magnitudes of C=O and -OH stretching bands shown on FT-IR spectrum of ATANC specimen are significantly larger than those of the ANC specimen, (see Figs. 1a and 1b). Presumably, the significant increase in the magnitude of C=O and -OH stretching bands observed for ATANC specimens is attributed to the newly added C=O and -OH functional groups exposed on etched surfaces of ATANC particles after acid treatment by H_2SO_4/HNO_3 solutions (1:3 v/v) for 40 minutes. After modification with $PE_{g\text{-}MAH}$, the peak magnitudes corresponding to C=O and -OH stretching bands of FANC specimens reduced significantly as the weight ratios of $PE_{g\text{-}MAH}$ to ATANC increased (see Figs. 1c to 1g). In fact, as shown in Figs. 1e to 1g, the C=O and -OH stretching band originally present in ANC and/or ATANC specimens disappeared almost completely as the weight ratios of $PE_{g\text{-}MAH}$ to ATANC of FANC specimens were equal to or more than 12.5. In the meantime, a new absorption band centered at around 1268 cm^{-1} corresponding to the motion of ester C-O stretching vibration[55] was found in the spectra of FANC^{m5}, FANC^{m10}, FANC$^{m12.5}$, FANC^{m15} and FANC^{m20} specimens (see Figs. 1c to 1g). In contrast, the absorption bands centered at

1710 and 1791 cm^{-1} corresponding to the motion of C=O and O-C=O stretching vibrations of maleic anhydride gradually reappeared as the weight ratios of $PE_{g\text{-}MAH}$ to ATANC were equal to or more than 15. Presumably, the gradual disappearance of C=O and -OH stretching bands and newly developed ester C-O stretching bands of $FANC^{mx}$ specimens is attributed to the reaction of the carboxylic and hydroxyl groups of ATANC specimens with the maleic anhydride groups of $PE_{g\text{-}MAH}$ molecules during their functionalized processes. The reappearance of O-C=O and C=O stretching bands of maleic anhydride groups is most likely due to the over-dosage of $PE_{g\text{-}MAH}$ during the functionalized processes of $FANC^{mx}$ specimens.

Morphological analysis of the original, acid treated and functionalized activated nanocarbons

Fig. 2 exhibits typical TEM micrographs of original, acid treated and functionalized activated nanocarbon (ANC, ATANC and $FANC^{mx}$) specimens. Typical irregular particle feature with dimensions of 20-120 nm in diameter was observed for the original ANC specimen (see Fig. 2a). After etching by H_2SO_4/HNO_3 solutions (1:3 v/v), a generalized rupture of ANC particles with dimensions of 10-60 nm in diameter, and the irregular ANC particles were significantly etched into broken and even smaller nanoparticles (see Fig. 2b). After being modified by $PE_{g\text{-}MAH}$, some translucent resins were found attaching on the surfaces of ANC particles, wherein the amounts of attached translucent resins increased gradually as the weight ratios of $PE_{g\text{-}MAH}$ to ATANC increased (see Figs. 2c to 2g). As evidenced by FT-IR analyses in the previous section, the attached translucent resins were most likely the grafted $PE_{g\text{-}MAH}$ molecules, which were firmly bonded to ATANC particles by the reaction of the maleic anhydride groups of $PE_{g\text{-}MAH}$ molecules with the carboxylic and hydroxyl groups of the ATANC particles. In fact, the translucent resins were found fully surrounding and overwrapping on ATANC particles, as the weight

ratios of $PE_{g\text{-}MAH}$ to ATANC are greater than 12.5.

Specific surface area analyses of ANC, ATANC and $FANC^{mx}$ particles

The values of specific surface areas of ANC, ATANC and $FANC^{mx}$ particles are summarized in table 1. The specific surface area of the ANC particles reached an extraordinary high value at 1047.4 $m^2 \cdot g^{-1}$. After acid treatment, the specific surface area of ATANC particles increased further to 1056.8 $m^2 \cdot g^{-1}$. This increase in specific surface area is attributed to newly exposed surfaces created on ATANC particles after etching by H_2SO_4/HNO_3 solutions (1:3 v/v) for 40 minutes. After modification by $PE_{g\text{-}MAH}$, the specific surface areas of $FANC^{mx}$ specimens increased significantly with the increase in weight ratios of $PE_{g\text{-}MAH}$ to ATANC and reached a maximal value at 1098.6 $m^2 \cdot g^{-1}$ as the weight ratios of $PE_{g\text{-}MAH}$ to ATANC approached an optimal value at 12.5. In contrast, the specific surface areas of the $FANC^{mx}$ specimens reduced from 1098.6 to 1071.3 and 987.4 $m^2 \cdot g^{-1}$, as the weight ratios of $PE_{g\text{-}MAH}$ to ATANC increased from 12.5 to 15 and 20, respectively. Presumably, the beneficial effect of $PE_{g\text{-}MAH}$ contents on specific surface areas of $FANC^{mx}$ specimens is attributed to the increase in grafted amounts and specific surface areas of $PE_{g\text{-}MAH}$ on ATANC specimens during their functionalized processes. However, $PE_{g\text{-}MAH}$ molecules may agglomerate, bundle, entangle together and overwrap the ATANC particles, as $PE_{g\text{-}MAH}$ molecules are superfluous and can no longer graft onto the ATANC nanoparticles. As evidenced by the morphology analysis in the previous section, some translucent resins were found fully surrounding and overwrapping on ATANC particles, as the weight ratios of $PE_{g\text{-}MAH}$ to ATANC were equal to or more than 15. Based on this premise, it is reasonable to infer that the overwrapped ATANC particles exhibit relatively lower specific surface areas than those $FANC^{mx}$ particles grafted with proper amounts of $PE_{g\text{-}MAH}$ resins.

Thermal properties of the as-prepared fibers

The melting temperature (T_m), crystallinity percentage (X_c) and evaluated lamellar thickness (l_c) values of UHMWPE (F_{100}), UHMWPE/ATANC ($F_{100}ATANC_y$) and UHMWPE/FANC ($F_{100}FANC^{mx}_y$) as-prepared fiber specimens are summarized in table 2. A main melting endotherm with a T_m and X_c at 142.7 ℃ and 65.1%, respectively, was found for the UHMWPE as-prepared fiber specimen (*i.e.* F_{100} specimen). After incorporation of ATANC and/or $FANC^{mx}$ particles in UHMWPE, T_m (or evaluated l_c) values of $F_{100}ATANC_y$ and $F_{100}FANC^{mx}_y$ as-prepared fiber series specimens reduced to a minimal value, but X_c values increased to a maximal value, as their ATANC and/or FANC contents reached 0.1 and 0.075 phr, respectively. In which, the T_m (or l_c) values of $F_{100}FANC^{mx}_y$ as-prepared fibers were significantly lower, but X_c values of $F_{100}FANC^{mx}_y$ as-prepared fibers were significantly higher than those of the corresponding $F_{100}ATANC_y$ as-prepared fibers with the same ATANC contents but without being functionalized. For instance, T_m values of $F_{100}FANC^{m5}_y$ as-prepared fibers reduced from 142.7 ℃ to 138.7 ℃ and to 137.7 ℃, but X_c values increased from 65.1% to 69.3% and to 72.6%, as their $FANC^{m5}$ contents increased from 0 to 0.025 and 0.075 phr, respectively. Moreover, it is worth noting that $F_{100}FANC^{m12.5}_{0.075}$ as-prepared fibers exhibited lower T_m (or l_c) but higher X_c values than those of other $F_{100}FANC^{mx}_{0.075}$ as-prepared fibers prepared with 0.075 phr optimal FANC content but modified with weight ratios of $PE_{g\text{-}MAH}$ to ATANC other than the optimal value at 12.5 (see table 2).

As evidenced by specific surface area and TEM analysis in the previous sections, the ATANC and FANC particles have extremely high surface areas per volume, which make them in close proximity to a large fraction of the UHMWPE matrix. Apparently, even very small contents of dispersed ATANC and FANC particles can serve as efficient

nucleation sites for UHMWPE molecules during their gel-spinning processes. These efficient nucleation sites of ATANC and FANC particles then facilitate the crystallization of UHMWPE molecules into crystals with thinner lamellar thickness and/or lower melting temperature values during their crystallization processes. In which, properly functionalized FANC particles with even higher specific surface areas are likely to disperse better in UHMWPE and serve as more effective sites for nucleation of UHMWPE molecules during their gel spinning processes than ANC and/or ATANC particles without being functionalized. As a consequence, $F_{100}FANC^{mx}{}_{y}$ as-prepared fibers exhibit significantly higher X_c but lower T_m (or evaluated l_c) values than those corresponding $F_{100}ATANC_y$ as-prepared fibers prepared with the same ATANC contents but without grafting with $PE_{g\text{-}MAH}$.

Orientation factor analysis of the as-prepared and drawn fiber specimens

Typical orientation factor (f_o) values of F_{100}, $F_{100}ATANC_y$ and $F_{100}FANC^{mx}{}_{y}$, as-prepared and drawn fiber specimens are summarized in Fig. 3. No significant difference in f_o values was found for F_{100}, $F_{100}ATANC_y$ and $F_{100}FANC^{mx}{}_{y}$ as-prepared fiber specimens. As expected, f_o values of F_{100}, $F_{100}ATANC_y$, and $F_{100}FANC^{mx}{}_{y}$ fiber specimens increased consistently as their draw ratios increased. After addition of ATANC and/or $FANC^{mx}$ particles, the f_o values of drawn $F_{100}ATANC_y$ and/or $F_{100}FANC^{mx}{}_{y}$ fiber specimens were significantly higher than those of drawn F_{100} fiber specimens with the same draw ratios. The f_o values of drawn $F_{100}ATANC_y$ fiber specimens with a fixed draw ratio reached a maximal value as their ATANC contents approached an optimal value at 0.1 phr. Similarly, f_o values of each drawn $F_{100}FANC^{mx}{}_{y}$ fiber series specimens reached a maximal value as their $FANC^{mx}$ contents approached an optimal value at 0.075 phr. In which, the f_o values of $F_{100}FANC^{mx}{}_{0.075}$ drawn fiber specimens

with 0.075 phr optimal FANC content were significantly higher than those of $F_{100}ATANC_{0.1}$ drawn fiber specimens with the same draw ratios but with 0.1 phr optimal ATANC content. Moreover, the maximal f_o values obtained for drawn $F_{100}FANC^{mx}{}_{0.075}$ fiber specimens prepared at 0.075 phr optimal $FANC^{mx}$ content reached another maximal value as the weight ratios of $PE_{g\text{-}MAH}$ to ATANC approached an optimal value at 12.5.

Achievable draw ratios of the as-prepared fiber specimens

Fig. 4 summarized the achievable draw ratio (D_{ra}) values of F_{100}, $F_{100}ATANC_y$ and $F_{100}FANC^{mx}{}_y$ as-prepared fiber specimens prepared at varying ATANC and FANC contents, respectively. For comparison purposes, D_{ra} values of the best prepared UHMWPE/functionalized carbon nanotube (UHMWPE/FCNT) and UHMWPE/ functionalized bacterial cellulose (UHMWPE/FBC) as-prepared fiber specimens obtained in our previous investigations[33, 38] were also included in Fig. 3. In which, bacterial cellulose nanofibers and carbon nanotubes are nanofillers with relatively high but significantly lower specific surface areas than that of the ANC particles used in this study (393.7 $m^2 \cdot g^{-1}$ and 100.5 $m^2 \cdot g^{-1}$ vs. 1047.4 $m^2 \cdot g^{-1}$). After addition with ATANC and/or $FANC^{mx}$ particles in UHMWPE, D_{ra} values of both $F_{100}ATANC_y$ and $F_{100}FANC^{mx}{}_y$ as-prepared fiber specimens reach a maximal value as their ATANC and/or $FANC^{mx}$ contents approach an optimal value at 0.1 and 0.075 phr, respectively, wherein the maximal D_{ra} values obtained for $F_{100}FANC^{mx}{}_{0.075}$ as-prepared fiber specimens prepared at varying $PE_{g\text{-}MAH}$/ATANC weight ratios are significantly higher than the maximal D_{ra} values obtained for the $F_{100}ATANC_{0.1}$ as-prepared fiber specimen prepared at 0.1 optimal ATANC content, respectively (see Fig. 4). It is worth noting that the maximal D_{ra} value obtained for the best prepared $F_{100}FANC^{m12.5}{}_{0.075}$ as-prepared fiber specimen prepared at 0.075 phr optimal $FANC^{m12.5}$ content are significantly higher than those of other

$F_{100}FANC^{mx}_{0.075}$ as-prepared fiber specimens prepared with weight ratios of $PE_{g\text{-}MAH}$ to $FANC^{mx}$ other than the optimal value at 12.5. As shown in Fig. 4, the maximal D_{ra} value obtained for $F_{100}FANC^{m12.5}_{0.075}$ as-prepared fiber specimen is about 4.5, 3.0 and 2.1 times of those of the best prepared UHMWPE, UHMWPE/FCNT and UHMWPE/FBC as-prepared fiber specimens prepared with the optimal FCNT and FBC contents.

As evidenced by thermal and lamellar thickness analyses, the T_m and/or evaluated l_c values of $F_{100}ATANC_y$ and $F_{100}FANC^{mx}_y$ as-prepared fiber specimens reduce significantly with the increase in ATANC and $FANC^{mx}$ contents, respectively, although the amounts of crystals with lower T_m and/or evaluated l_c values increase significantly as the ATANC and/or $FANC^{mx}$ contents increase to an optimal value, respectively. Presumably, these crystals with lower T_m and/or evaluated l_c values can be melted and/or pulled out of folded lamellar crystals relatively easily during the ultradrawing processes, and hence, results in higher drawability and orientation of the $F_{100}ATANC_y$ and $F_{100}FANC^{mx}_y$ fiber specimens. However, the amounts of coagulated ATANC and/or $FANC^{mx}$ particles are likely to increase significantly when their ATANC and/or $FANC^{mx}$ contents are higher than certain values, respectively. These coagulated ATANC and/or $FANC^{mx}$ particles can slide against each other and serve as the defects for stress concentration during the drawing processes of $F_{100}ATANC_y$ and $F_{100}FANC^{mx}_y$ as-prepared fiber specimens, and hence, lead to an early breakage and/or significant reduction in D_{ra} values of the resulted drawn fibers. Based on these premises, it is reasonable to understand that the D_{ra} values of $F_{100}ATANC_y$ and $F_{100}FANC^{mx}_y$ as-prepared fiber specimens reduce significantly when their ATANC and/or $FANC^{mx}$ contents are higher than the specific optimal value, respectively.

Dynamic mechanical properties of the as-prepared fiber specimens

Fig. 5 summarized the temperature dependence of the storage modulus (E') and tan δ

of F_{100} and $F_{100}FANC^{m12.5}{}_{y}$ as-prepared fiber specimens. Three distinct transitions (i.e. α-, β- and γ- transitions) were observed at temperatures near 90 to 130℃, -45 to -15 ℃ and -120 ℃ in the tan δ curves of F_{100} and $F_{100}FANC^{m12.5}{}_{y}$ as-prepared fiber specimens, respectively. It is interesting to note that the *α*- and *β*- transition temperatures of the $F_{100}FANC^{m12.5}{}_{y}$ as-prepared fiber specimens reduce significantly from 130 to 90 ℃ and -15 to -45 ℃, respectively, as their $FANC^{m12.5}$ contents increase from 0 to 0.075 phr. At $FANC^{m12.5}$ contents ≧ 0.075 phr, *α*- and *β*-transition temperatures of $F_{100}FANC^{m12.5}{}_{y}$ as-prepared fiber specimens increase significantly from 90 to 100 ℃ and -45 to -30 ℃, respectively, as their $FANC^{m12.5}$ contents increase from 0.075 to 0.125 phr. In contrast, the *γ*-transition temperatures of $F_{100}FANC^{m12.5}{}_{y}$ as-prepared fiber specimens remain relatively unchanged as their $FANC^{m12.5}$ contents increase from 0 to 0.075 and 0.125 phr.

The relaxation processes of melt-crystallized polyethylene resins with regular molecular weights have been extensively studied[56-64]. The *β*- and *γ*-transitions at temperatures near -20 and -120 ℃ are attributed to the motion of branches[59-62] and the crankshaft motion of short polymer segments requiring a minimum of three methylene units[58, 63, 64] in the amorphous matrix, respectively. In contrast, the *α*-transition at temperatures near 40-60 ℃ is generally ascribed to motions or deformations in the interfacial region (tie molecules, loops, folds, etc.), that originate from chain mobility in the crystals[58]. Based on these premises, the transitions found at peak temperatures near -120 ℃ can be attributed to the γ-transition of UHMWPE molecules of the F_{100} and $F_{100}FANC^{m12.5}{}_{y}$ as-prepared fiber specimens with varying $FANC^{m12.5}$ contents.

The transitions that occurred at peak temperatures near 90 to 130 ℃ are attributed to the molecular motions associated with the *α*-transitions of UHMWPE molecules, although the observed transition temperatures are significantly higher than the *α*-transition

temperatures of melt-crystallized polyethylenes with regular molecular weights. Presumably, the particularly high α-transition temperatures found for F_{100} and $F_{100}FANC^{m12.5}{}_{y}$ as-prepared fiber specimens are possibly due to their specific interfacial microstructures crystallized from UHMWPE and/or UHMWPE/$FANC^{m12.5}{}_{y}$ gel solutions. The molecular motions or deformations in the interfacial region originated from UHMWPE crystals may be much more difficult than those originated from melt-crystallized polyethylene crystals with regular molecular weights, because the restrained chain mobility resulted from extraordinary long UHMWPE molecules in the crystal and interfacial regions are much higher than those from regular polyethylene molecules. On the other hand, as evidenced by DSC analysis, melting temperatures of the $F_{100}FANC^{m12.5}{}_{y}$ as-prepared fibers reduce significantly to a minimal value as their $FANC^{m12.5}$ contents reach the optimal value at 0.075 phr. The molecular motions or deformations in interfacial regions of the possibly less perfect UHMWPE crystals with lower melting temperatures of $FANC^{m12.5}$ contained $F_{100}FANC^{m12.5}{}_{y}$ as-prepared fiber specimens are expected to be relatively easier than those resulted from the boundary regions of more perfect UHMWPE crystals with significantly higher melting temperatures. As a consequence, the lowest temperature is required to motivate the molecular motions of UHMWPE resulted from α-transitions of the $F_{100}FANC^{m12.5}{}_{0.075}$ as-prepared fiber specimens prepared at the optimal $FANC^{m12.5}$ content at 0.075 phr.

Finally, the transitions found at peak temperatures near -45 to -15 ℃ of $F_{100}FANC^{m12.5}{}_{y}$ as-prepared fiber specimens are most likely due to the molecular motions associated with the β-transitions of UHMWPE molecules, although some of the β-transition temperatures are significantly lower than the β-transition temperatures (*c.a.* -20 ℃) generally found for melt-crystallized polyethylenes with regular molecular weights[59-62]. As mentioned previously, even small contents of activated nanocarbon

particles can serve as efficient nucleation sites and facilitate the crystallization of UHMWPE molecules into possibly poor crystals with low melting temperatures during the gel-spinning processes of $F_{100}FANC^{m12.5}{}_{y}$ fibers. Presumably, during such rapid nucleation processes, the UHMWPE molecules (especially in the branch parts) remaining in the amorphous regions may solidify and pack relatively randomly without being well structured. Accordingly, it is reasonable to understand that the branch motions derived from the amorphous regions of $F_{100}FANC^{m12.5}{}_{y}$ as-prepared fiber specimens become much easier, when they were prepared at the optimal $FANC^{m12.5}$ contents at 0.075 phr.

Tensile properties

Tensile strength (σ_f) and modulus (E) values of F_{100}, $F_{100}ATANC_y$ and $F_{100}FANC^{mx}{}_{y}$ as-prepared fiber specimens prepared at varying draw ratios are illustrated in Fig. 6. For comparison purposes, σ_f and E values of the best prepared UHMWPE/functionalized carbon nanotube (UHMWPE/FCNT) and UHMWPE/functionalized bacterial cellulose (UHMWPE/FBC) as-prepared fiber specimens obtained in our previous investigations [33, 38] were also summarized in Fig. 6. As expected, σ_f and E values of the drawn F_{100}, UHMWPE/FCNT, UHMWPE/FBC, $F_{100}ATANC_y$ and $F_{100}FANC^{mx}{}_{y}$ fiber specimens improve consistently as their draw ratios increase. It is worth noting that σ_f and E values of the best prepared UHMWPE/FCNT, UHMWPE/FBC drawn fiber specimens and/or any $F_{100}ATANC_y$ and $F_{100}FANC^{mx}{}_{y}$ drawn fiber specimens are significantly higher than those of the corresponding drawn F_{100} fiber specimen with the same draw ratio but without addition of any nanofiller. In which, σ_f and E values of the drawn $F_{100}FANC^{mx}{}_{y}$ fiber specimens are significantly higher than those of the best prepared UHMWPE/FCNT or UHMWPE/FBC drawn fiber specimens with the same draw ratios but without addition of $FANC^{mx}$ particles with extraordinary high specific surface areas. Similar to those

found for their f_o values, σ_f and E values of each drawn $F_{100}ATANC_y$ and $F_{100}FANC^{mx}{}_y$ fiber series specimens with a fixed draw ratio approach a maximal value as their ATANC and $FANC^{mx}$ contents near an optimal value at 0.1 and 0.075 phr, respectively. In which, the maximal σ_f and E values of $F_{100}FANC^{mx}{}_{0.075}$ fiber specimens are significantly higher than that of the $F_{100}ATANC_{0.1}$ fiber specimen with the same draw ratios and contents of ATANC particles without grafting with $PE_{g\text{-}MAH}$ resins. Moreover, it is worth noting that the maximal σ_f and E values obtained for the drawn $F_{100}FANC^{m12.5}{}_{0.075}$ fiber specimens are significantly higher than those of other $F_{100}FANC^{mx}{}_{0.075}$ fiber specimens prepared at the same draw ratio and 0.075 phr $FANC^{mx}$ content but modified with weight ratios of $PE_{g\text{-}MAH}$ to ATANC other than the optimal value at 12.5. As shown in Fig. 6, the ultimate tensile strength value of the best prepared $F_{100}FANC^{m12.5}{}_{0.075}$ drawn fiber prepared using one-stage drawing process at 95 ℃ reached 7.8 GPa, which is about 2.9, 1.34 and 1.1 times of those of the best prepared UHMWPE, UHMWPE/functionalized CNT and UHMWPE/modified bacterial cellulose drawn fibers, respectively, that were prepared at the same optimal UHMWPE concentration and drawing condition but without or addition of nanofillers with significantly lower specific surface areas.

The mechanical properties of the drawn specimens are generally believed to depend mainly upon the degree of orientation of the drawn specimens as their molecular weights are constant[23, 65]. As evidenced by the orientation analysis in the previous section, at a fixed draw ratio, the f_o values of $F_{100}ATANC_{0.1}$ and $F_{100}FANC^{mx}{}_{0.075}$ drawn fiber specimens prepared at the optimal ATANC and $FANC^{mx}$ contents, respectively, are always higher than those of other $F_{100}ATANC_y$ and/or $F_{100}FANC^{mx}{}_y$ drawn fiber specimens prepared with ATANC and/or $FANC^{mx}$ contents deviating from their optimal values, respectively. In which, the f_o values of the $F_{100}FANC^{m12.5}{}_{0.075}$ drawn fiber specimens are always higher than those of other $F_{100}FANC^{mx}{}_{0.075}$ drawn fiber specimens prepared with

the same draw ratios and $FANC^{mx}$ contents but modified using weight ratios of $PE_{g\text{-}MAH}$ to ATANC other than the optimal value at 12.5. These results clearly suggest that a good orientation of UHMWPE molecules along the drawing direction positively affects the tensile properties of the F_{100}, $F_{100}ATANC_y$ and $F_{100}FANC^{mx}{}_y$ fiber specimens. Excellent orientation and ultimate tensile properties of the UHMWPE/nanofiller fibers can be prepared by ultradrawing the $F_{100}FANC^{mx}{}_y$ as-prepared fibers with optimal contents of $FANC^{mx}$ particles well dispersing in the as-prepared fibers. In fact, the best prepared $F_{100}FANC^{m12.5}{}_{0.075}$ dawn fibers filled with nanoparticles with extraordinary high specific surface area (*c.a.* 1100 m^2/g) exhibited an extremely high σ_f value at 7.8 GPa, which is the highest σ_f value obtained so far for UHMWPE/nanofiller composite fibers prepared in our investigations[31-38]. This value is about 190%, 34% and 10% higher than those of the best prepared UHMWPE, UHMWPE/functionalized CNT and UHMWPE/modified bacterial cellulose drawn fiber specimens, respectively, prepared in our previous investigations. Apparently, well dispersed functionalized nanofillers with higher specific surface areas in UHMWPE/functionalied nanofiller fibers can positively affect their ultradrawing, orientation and ultimate tensile properties.

Conclusion

This investigation presents a novel way to improve the ultradrawing and ultimate tensile properties of UHMWPE fibers by incorporating very small amounts of nucleation nanofillers during the gel spinning process of UHMWPE fibers. Original, acid treated and functionalized activated nanocarbons with specific surface areas higher than 1000 $m^2 \cdot g^{-1}$ were added into the UHMWPE fibers as effective nucleation nanofillers for the first time in the literature. As a result, T_m and evaluated l_c values of $F_{100}ATANC_y$ and $F_{100}FANC^{mx}{}_y$ as-prepared fiber series specimens reduce, but X_c values increase significantly as their ATANC and $FANC^{mx}$ contents increase to an optimal value at 0.1 and 0.075 phr, respectively. The $F_{100}FANC^{m12.5}{}_y$ fiber specimens exhibit an extraordinarily high α- but low β-transitions, in which the peak temperatures of α- and β-transitions reduce significantly when their $FANC^{m12.5}$ contents increase to an optimal value at 0.075 phr. Similar to the improvement in the achievable draw ratios of $F_{100}ATANC_y$ and $F_{100}FANC^{mx}{}_y$ as-prepared fibers, the f_o, σ_f and E values of $F_{100}ATANC_y$ and $F_{100}FANC^{mx}{}_y$ drawn fibers with a fixed draw ratio approached a maximal value as the ATANC and $FANC^{mx}$ contents reached an optimal value at 0.1 and 0.075 phr, respectively. The best prepared $F_{100}FANC^{m12.5}{}_{0.075}$ dawn fiber filled with $FANC^{m12.5}$ particles of the highest specific surface area (*c.a.* 1100 m^2/g) yield an extraordinary high ultimate σ_f at 7.8 GPa, which is the highest σ_f value reported so far in the literature. This value is about 190%, 34% and 10% higher than those of the best prepared UHMWPE, UHMWPE/functionalized CNT and UHMWPE/modified bacterial cellulose drawn fiber specimens, respectively, prepared in our previous investigations. These results clearly suggest that well dispersed functionalized nanofillers with higher specific surface areas in UHMWPE/functionalied nanofiller fibers can positively affect their ultradrawing, orientation and ultimate tensile properties.

ACKNOWLEDGEMENTS

The authors would like to express their appreciation to the Department of Industrial Technology, Ministry of Economic Affairs (99-EC-17-A-11-S1-155 and 100-EC-17-A-11-S1-155) and National Science Council (NSC 99-2221-E-011-010-MY3 and NSC 102-2221-E-168-038-MY3) for support of this work.

Notes and References

1. T. Kajiwara and J.E. Mcintyre, Advanced Fiber Spinning Technology. Chap 8. Woodhead, Publishing Ltd: Cambridge. 1994: 174.
2. P. Smith and P.J. Lemstra, *Macromol. Chem. Phys.*, 1979; 180, 2983-2986.
3. P.J. Barham and A. Keller, *J. Mater. Sci.*, 1985, 20, 2281-2302.
4. P. Smith and P.J. Lemstra, *J. Mater. Sci.*, 1980; 15, 505-514.
5. Technical Textiles International, 1996; 4: 3.
6. C. Li, Y. Zhang and Y. Zhang, *Polym. Test*, 2003, 22, 191-195.
7. O. Darras, R. Sequela and F. Rietsch, *J. Polym. Sci. Polym. Phys. Ed*, 1992, 30, 349-359.
8. J.T. Yeh and S.S. Chang, *J. Mater. Sci.*, 2000, 35, 3227-3236.
9. J.T. Yeh, S.S. Chang and M.S. Yen, *J. Appl. Polym. Sci.*, 1998, 70, 149-159.
10. J.T. Yeh and S.S. Chang, *Polym. Eng. Sci.*, 2002, 42, 1558-1567.
11. J.T. Yeh and S.S. Chang, *J. Appl. Polym. Sci.*, 2001, 79, 1890-1901.
12. J.T. Yeh, Y.L. Lin, and C.C. Fan-Chiang, *Macromol. Chem. Phys.*, 1996, 197, 3531-3540.
13. J.T. Yeh and H.C. Wu, *Polym. J.*, 1998, 30, 1-10 .
14. J.T. Yeh, Y.T. Lin and H.B. Jiang, *J. Appl. Polym. Sci.*, 2003, 91, 1559-1570.
15. J.T. Yeh, Y.T. Lin and K.N. Chen, *J. Polym. Res.*, 2003, 10, 55-63.
16. J.T. Yeh, Y.T. Lin and K.N. Chen, *J. Appl. Polym. Sci.*, 2003, 89, 3728-3738.

17. P. Smith, H.D. Chanzy and B.P. Rotzinger, *Polym. Commun.*, 1985, 26, 258-260.

18. P. Smith, H.D. Chanzy and B.P. Rotzinger, *J. Mater. Sci.*, 1987, 22, 523-531.

19. M. Matsuo, C. Sawatari, M. Iida and M. Yoneda, *Polym. J.*, 1985, 17, 1197-1208.

20. T. Kanamoto, A. Tsurta, K. Tanana, M. Takeda and R.S. Porter, *Macromolecules*, 1988, 21, 470-477.

21. J. Smook and A.J. Pennings, *J. Appl. Poly. Sci.*, 1982, 27, 2209-2228.

22. T. Jian, W.D. Shyu, Y.T. Lin, K.N. Chen and J.T. Yeh, *Polym. Eng. Sci.*, 2003, 43, 1765-1777.

23. T.Ohta, *Polym. Eng. Sci.*, 1983, 23, 697-703.

24. D.C. Prevorsek, Polymer liquid crystals. Academic Press: London. 1982.

25. B. Kalb and A.J. Pennings, *Polymer*, 1980, 21, 3-4.

26. M.A. Wilding and I.M. Word, *Polymer*, 1978, 19, 969-976.

27. P. Smith and P.J. Lemstra, *Polymer*, 1980, 21, 1341-1343.

28. S. Kavesh and D.C. Prevorsek, US Patent 4536536, 1985.

29. S. Kavesh and D.C. Prevorsek, US Patent 4551296, 1985.

30. S. Kavesh and D.C. Prevorsek, US Patent 4413110, 1983.

31. J.T. Yeh, C.W. Du, S.C. Lin, K.H. Hsie and F.C. Chang, *J. Mater. Sci.*, 2008, 43, 4892-4900.

32. J.T. Yeh, T.W. Wu, Y.C. Lai, Q.C. Li, H.P. Zhou, Q. Zhou, C.H. Tsou, Y.C. Shu, C.Y. Huang and K.S. Huang, *Polym. Eng. Sci.*, 2011, 51, 2552-2563.

33. J.T. Yeh, T.W. Wu, Y.C. Lai, H.P. Zhou, Q. Zhou, Q.C. Li, S. Wen, F.C. Tsai, C.Y. Huang, K.S. Huang and K.N. Chen, *Polym. Eng. Sci.*, 2011, 51, 687-696.

34. J.T. Yeh, S.C. Lin, K.N. Chen and K.S. Huang, *J. Appl. Polym. Sci.*, 2008, 110, 2538-2548.

35. J.T. Yeh, Y.C. Lai, H. Liu, Y.C. Shu, C.Y. Huang, K.S. Huang, and K.N. Chen,

Polym. Int., 2010, 60, 59-68.

36. J.T. Yeh, C.K. Wang, P. Hu, Y.C. Lai and F.C. Tsai, *Polym. Int.*, 2012, 61, 982-989.
37. J.T. Yeh, C.K. Wang, A. Yeh, L.K. Huang, W.H. Wang, K.H. Hsieh, C.Y. Huang and K.N. Chen, *Polym. Int.*, 2013, 62, 591-600.
38. J.T. Yeh, C.C. Tsai, C.K. Wang, J.W. Shao, M.Z. Xiao and S.C. Chen, *Carbonhyd. Polym.*, 2014, 101, 1-10.
39. G.A. Harpell, S. Kavesh, I. Palley and D.C. Prevorsek, US Patent 4455273, 1984.
40. M.I. Abo, E.I. Maaty, R.H. Olley and D.C. Bassett, *J. Mater. Sci.*, 1999, 34, 1975-1989.
41. M. Mastuo, C. Sawatari and T. Nakano, *Polym. J.*, 1986, 18, 759-774.
42. K. Yamaura, M. Suzuki, M. Yamamoto, R. Shimada and T. Tanigami, *J. Appl. Polym. Sci.*, 1995, 58, 1787-1791.
43. X.F. Zhang, L. Tao, T.V. Sreekumar, K. Satish, X. Hu and K. Smith, *Polymer*, 2004, 45, 8801-8807.
44. S.B. Kayiran, F.D. Lamari and D. Levesque, *J. Phys. Chem. B*, 2004, 108, 15211-15215.
45. A. Swiatkowski, M. Pakula and S. Biniak. *Electrochimica Acta*, 1997, 42, 1441-1447.
46. K. Kinoshita, *Carbon*. New York: Wiley. 1988: 110.
47. S. Timura, I.C. Kantarlib, S. Onenca and J. Yanika, *J. Anal. Appl. Pyrol.*, 2010, 89, 129-136.
48. T. Travinskaya, A. Perekhrest, Y. Savelyev, N. Kanellopoulos, K. Papadopoulos and K. Agiamarnioti, *Appl. Surf. Sci.*, 2010, 256, 4391-4396.
49. G.Q. Lu and D.D. Do, *Sep. Purif. Technol.*, 1993, 3, 106-110.
50. J.D. Hoffman and R.L. Miller, *Polymer*, 1997, 38, 3151-3212.
51. J.D. Hoffman and J.J. Weeks, *J. Res. Natl. Bur. Stand.*, 1962, 66, 13-28.

52. C. Xiao, Y. Zhang, S. An and G. Jia, *J. Appl. Polym. Sci.*, 1996, 59, 931-935.

53. T. Ramanathan, F.T. Fisher, R.S. Ruoff and L.C. Brinson, *Chem. Mater.*, 2005, 17, 1290-1295.

54. C. Toles, S. Rimmer and J.C. Hower, *Carbon*, 1996, 34, 1419-1426.

55. D.A. Skoog and J.J. Leary, *Principles of Instrumental Analysis*,*4th Ed.* Saunders: College. 1992: 279.

56. F. Fontaine, J. Ledent, G. Groeninckx and H. Reynaers, *Polymer*, 1982, 23, 185-191.

57. R.H. Boyd, *Polymer*, 1985, 26, 1123-1133.

58. Y.P. Khanna, E.A. Turi, T.J. Taylor, V.V. Vickroy and R.Y. Abbot, *Macromolecules*, 1985, 18, 1302-1309.

59. D.R. Saini and A.V. Shenoy, *Polym. Commun.*, 1985, 26, 50.

60. F.C. Stehling and L. Mandelkern, *Macromolecules*, 1970, 3, 242-252.

61. D.E. Kline and J.A. Saver, *J. Polym. Sci.*, 1956, 22, 455-462.

62. L.E. Nielson, *Mechanical Properties of Polymers.* New York: Reinhold. 1962: 180.

63. S.D. Clas, D.C. McFaddin and K.E. Russell, *J. Polym. Sci. Part B: Polym. Phys.*, 1987, 25, 1057-1069.

64. N.G. McCrum, B.E. Read and G. Williams, *Anelastic and Dielectric Effect in Polymeric Solids*. New York: Wiley. 1967: 1061.

65. W. Hoogsteen, G.T. Brinke and A.J. Pennings, *Colloid. Polym. Sci.*, 1988, 266, 1003-1013.

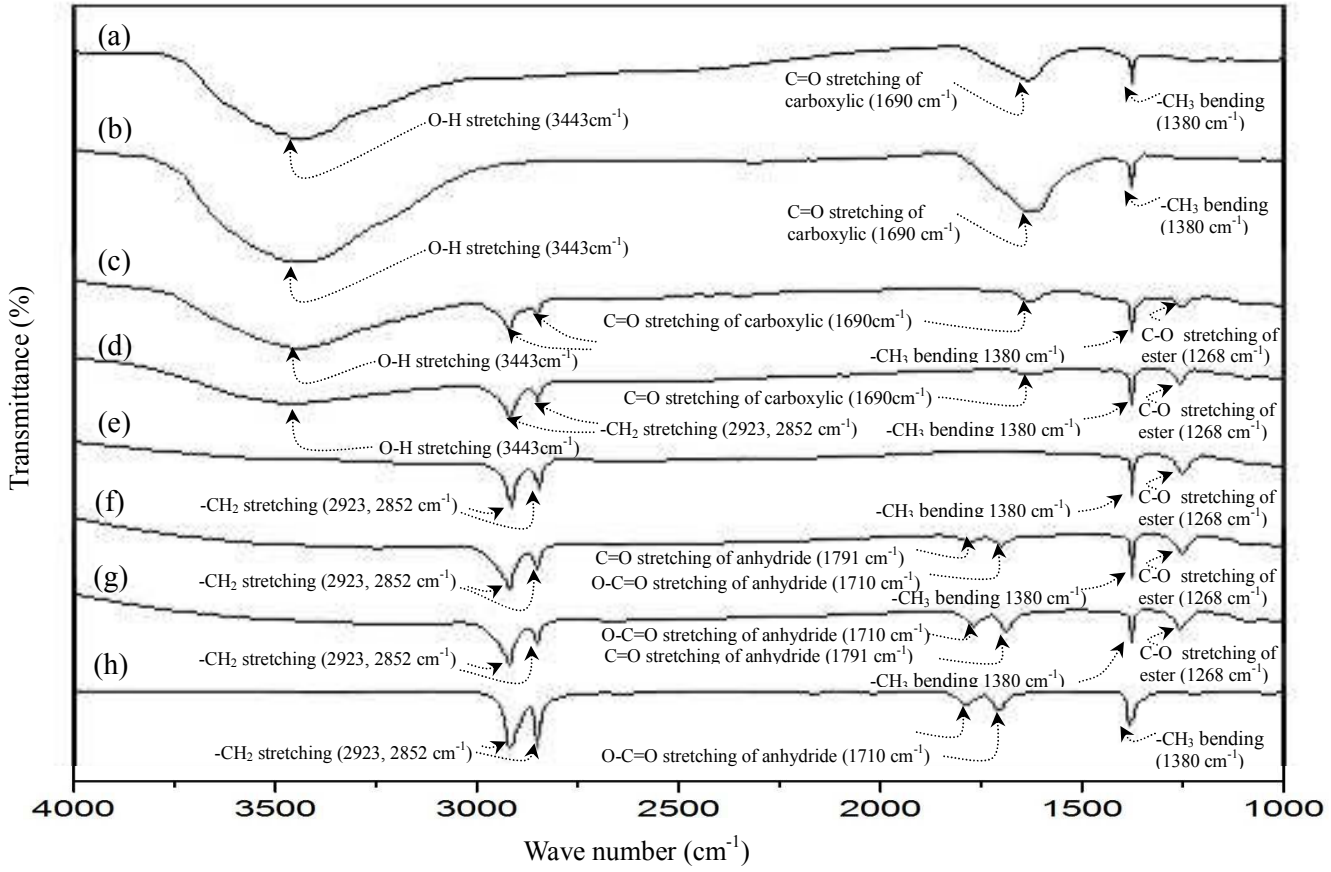

Figure 1 FT-IR spectra of (a) ANC, (b) ATANC, (c) FANC^{m5}, (d) FANC^{m10}, (e) FANC$^{m12.5}$, (f) FANC^{m15}, (g) FANC^{m20} and (h) PE$^{g\text{-}MAH}$ specimens.

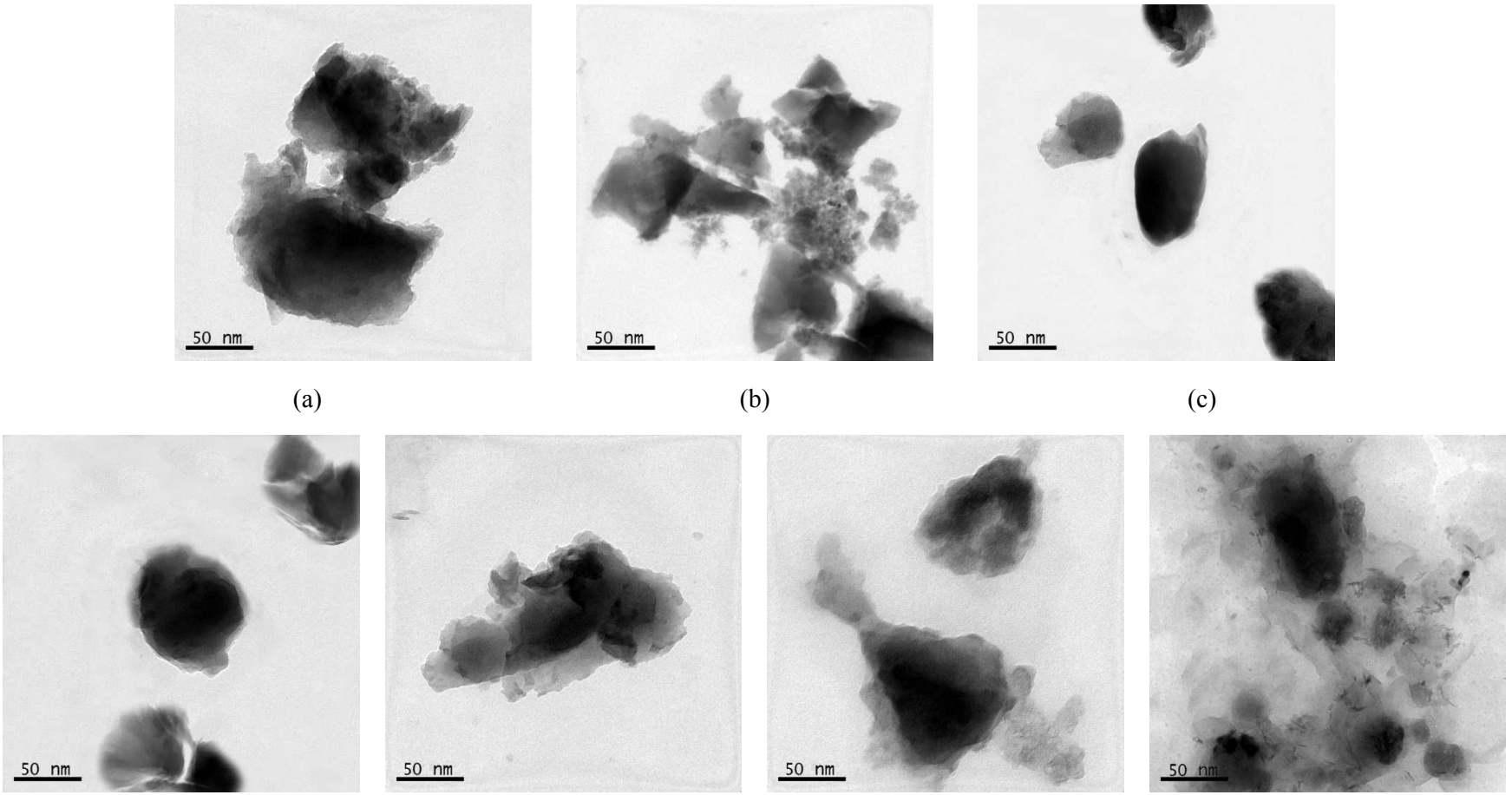

Figure 2 TEM micrographs of (a) ANC, (b) ATANC, (c) FANC^{m5}, (d) FANC^{m10}, (e) FANC$^{m12.5}$, (f) FANC^{m15} and (g) FANC^{m20} specimens.

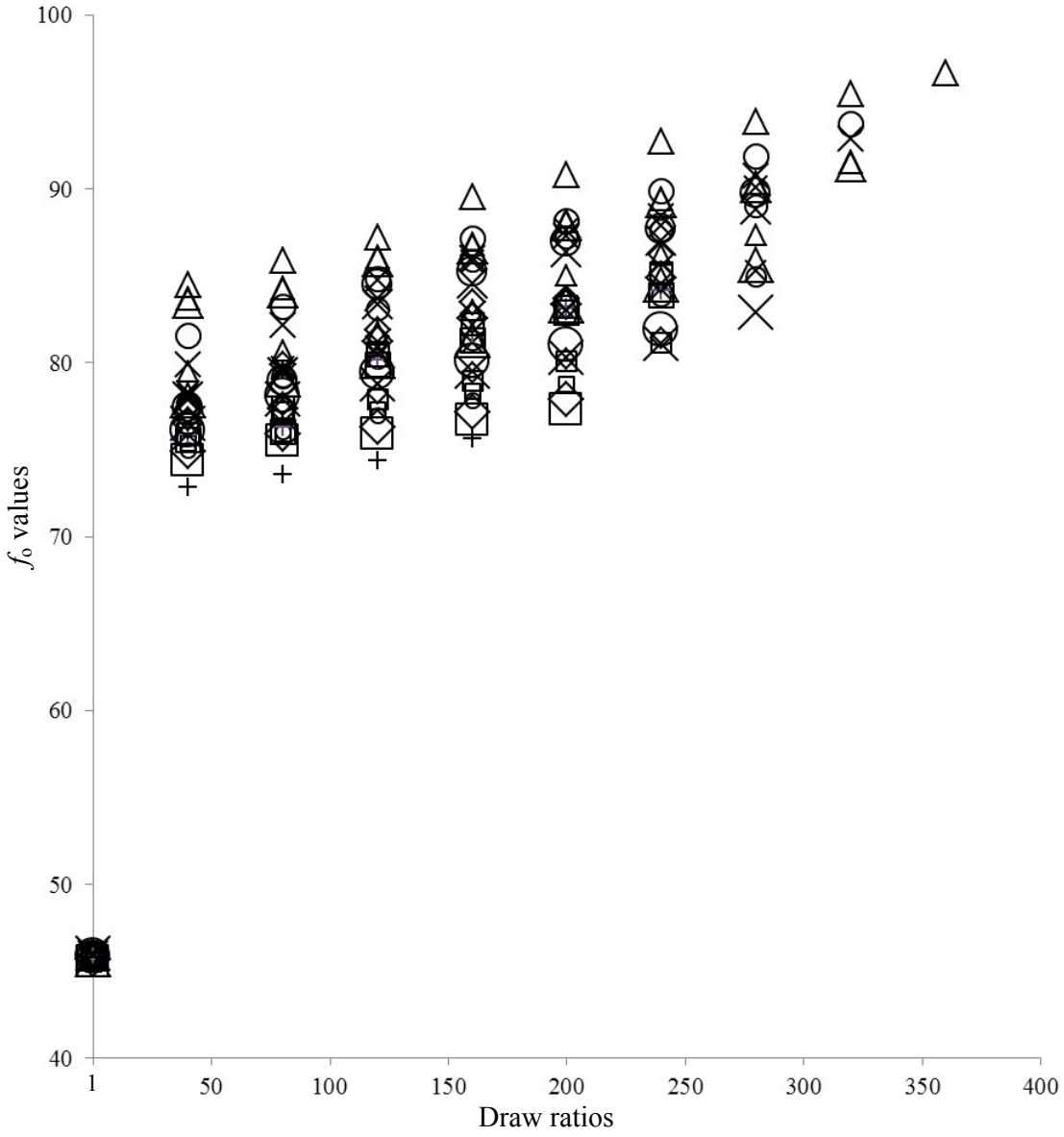

Figure 3 The orientation factor (f_0) values of F_{100} (+), $F_{100}ATANC_{0.025}$ (□), $F_{100}ATANC_{0.05}$ (◇), $F_{100}ATANC_{0.075}$ (△), $F_{100}ATANC_{0.1}$ (×), $F_{100}ATANC_{0.125}$ (○), $F_{100}FANC^{m5}{}_{0.025}$ (□), $F_{100}FANC^{m5}{}_{0.05}$ (◇), $F_{100}FANC^{m5}{}_{0.075}$ (△), $F_{100}FANC^{m5}{}_{0.1}$ (×), $F_{100}FANC^{m5}{}_{0.125}$ (○), $F_{100}FANC^{m10}{}_{0.025}$ (□), $F_{100}FANC^{m10}{}_{0.05}$ (◇), $F_{100}FANC^{m10}{}_{0.075}$ (△), $F_{100}FANC^{m10}{}_{0.1}$ (×), $F_{100}FANC^{m10}{}_{0.125}$ (○), $F_{100}FANC^{m12.5}{}_{0.025}$ (□), $F_{100}FANC^{m12.5}{}_{0.05}$ (◇), $F_{100}FANC^{m12.5}{}_{0.075}$ (△), $F_{100}FANC^{m12.5}{}_{0.1}$ (×), $F_{100}FANC^{m12.5}{}_{0.125}$ (○), $F_{100}FANC^{m15}{}_{0.025}$ (□), $F_{100}FANC^{m15}{}_{0.05}$ (◇), $F_{100}FANC^{m15}{}_{0.075}$ (△), $F_{100}FANC^{m15}{}_{0.1}$ (×), $F_{100}FANC^{m15}{}_{0.125}$ (○), $F_{100}FANC^{m20}{}_{0.025}$ (□), $F_{100}FANC^{m20}{}_{0.05}$ (◇), $F_{100}FANC^{m20}{}_{0.075}$ (△), $F_{100}FANC^{m20}{}_{0.1}$ (×) and $F_{100}FANC^{m20}{}_{0.125}$ (○) as-prepared and drawn fiber specimens with varying draw ratios.

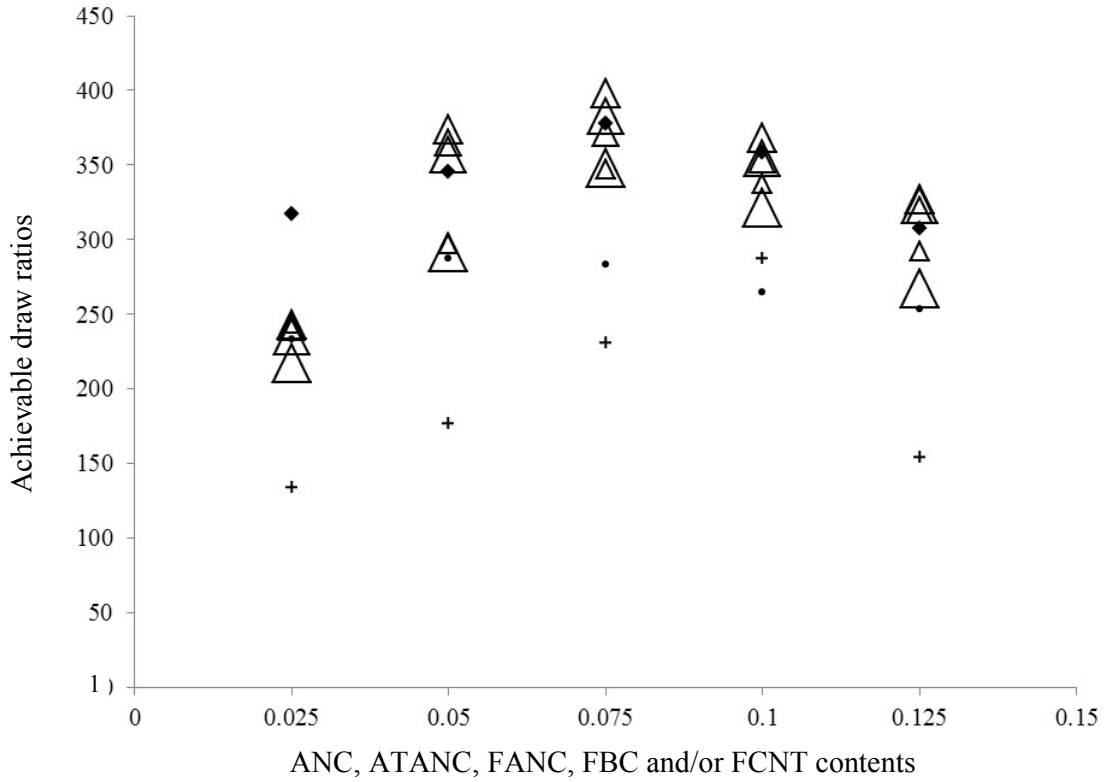

Figure 4 Achievable draw ratios of F_{100} (▪), the best prepared $F_{100}FCNT_y$ (•), the best prepared $F_{100}FBC_y$ (◆), $F_{100}ATANC$ (+),$F_{100}FANC^{m5}{}_y$ (△), $F_{100}FANC^{m10}{}_y$ (△), $F_{100}FANC^{m12.5}{}_y$ (△), $F_{100}FANC^{m15}{}_y$ (△) and $F_{100}FANC^{m20}{}_y$ (△) as-prepared fiber specimens.

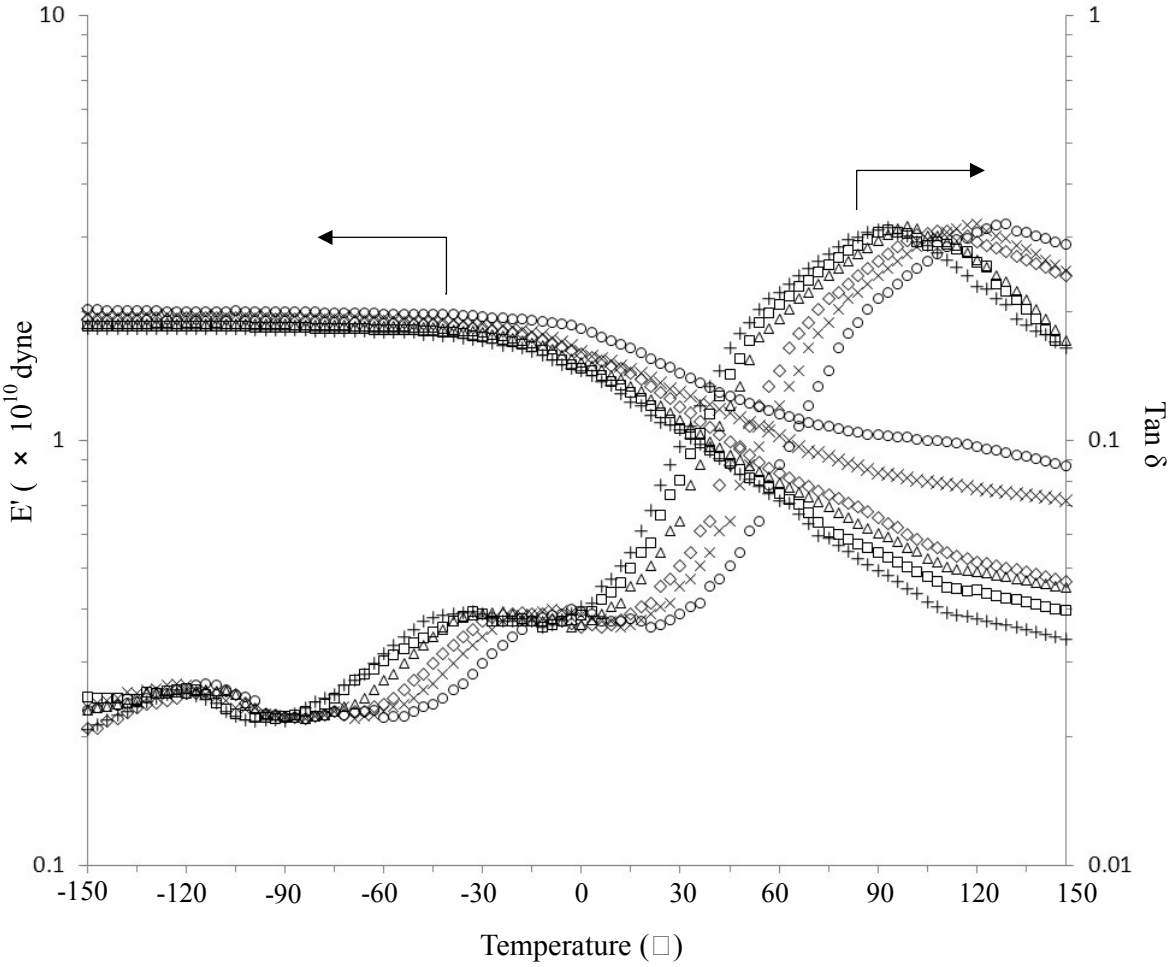

Figure 5 Plots of E' and tan δ as a function of temperature for F_{100} (○), $F_{100}FANC^{m12.5}{}_{0.025}$ (×), $F_{100}FANC^{m12.5}{}_{0.05}$ (□), $F_{100}FANC^{m12.5}{}_{0.075}$ (+), $F_{100}FANC^{m12.5}{}_{0.1}$ (△) and $F_{100}FANC^{m12.5}{}_{0.125}$ (◇) as-prepared fibers scanned at 1 Hz and a heating rate of 2 ℃/min.

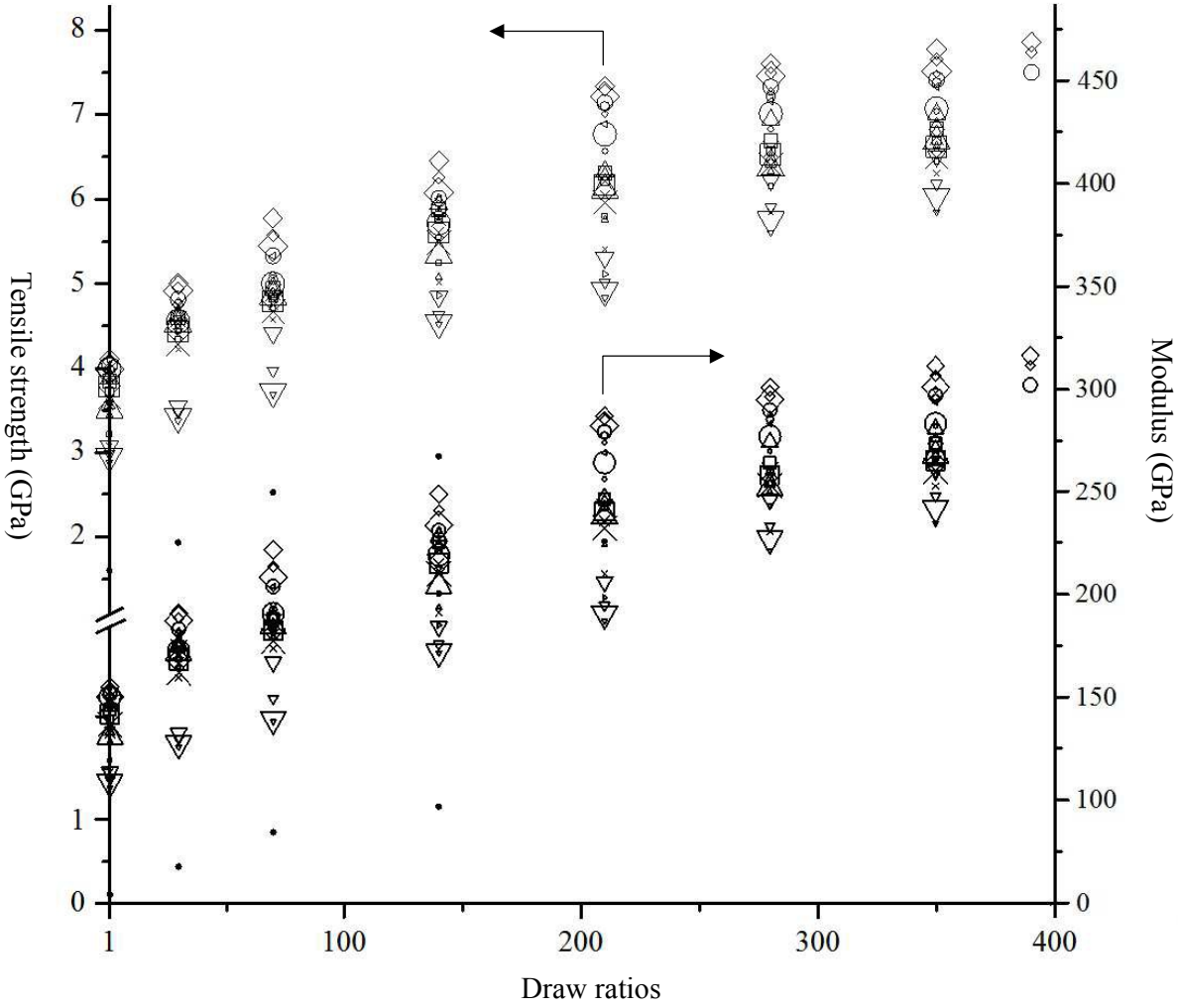

Figure 6 Tensile strength and modulus values of F_{100} (•, •), the best prepared UHMWPE/FCNT (◁,◁),the best prepared UHMWPE/FBC (▷, ▷), $F_{100}ATANC_{0.025}$(▽, ▽), $F_{100}ATANC_{0.05}$(▽, ▽), $F_{100}ATANC_{0.075}$(▽, ▽), $F_{100}ATANC_{0.125}$(▽, ▽), $F_{100}FANC^{m5}{}_{0.025}$ (▫, ▫), $F_{100}FANC^{m5}{}_{0.05}$ (□, □), $F_{100}FANC^{m5}{}_{0.075}$ (□, □), $F_{100}FANC^{m5}{}_{0.125}$ (□, □), $F_{100}FANC^{m10}{}_{0.025}$ (○, ○), $F_{100}FANC^{m10}{}_{0.05}$ (○, ○), $F_{100}FANC^{m10}{}_{0.075}$ (○, ○), $F_{100}FANC^{m10}{}_{0.125}$ (○, ○), $F_{100}FANC^{m12.5}{}_{0.025}$ (◇, ◇), $F_{100}FANC^{m12.5}{}_{0.05}$ (◇, ◇), $F_{100}FANC^{m12.5}{}_{0.075}$ (◇, ◇), $F_{100}FANC^{m12.5}{}_{0.125}$ (◇, ◇), $F_{100}FANC^{m15}{}_{0.025}$ (△, △), $F_{100}FANC^{m15}{}_{0.05}$ (△, △), $F_{100}FANC^{m15}{}_{0.075}$ (△, △), $F_{100}FANC^{m15}{}_{0.125}$ (△, △), $F_{100}FANC^{m20}{}_{0.025}$ (×, ×), $F_{100}FANC^{m20}{}_{0.05}$ (×, ×), $F_{100}FANC^{m20}{}_{0.075}$ (×, ×) and $F_{100}FANC^{m20}{}_{0.125}$ (×, ×) fiber specimens with varying draw ratios.

Table 1 Designations and specific surface areas of ANC, ATANC and FANC^{mx} particles

ANC, ATANC and FANC^{mx} particles	Mass ratios of $PE_{g\text{-}MAH}$ to ATANC used in functionalization experiments of FANC^{mx} particles	Specific surface areas ($m^2\ g^{-1}$)
ANC	--	1047.4
ATANC	--	1056.8
FANC^{m5}	5.0	1063.2
FANC^{m10}	10.0	1086.9
FANC$^{m12.5}$	12.5	1098.6
FANC^{m15}	15.0	1071.3
FANC^{m20}	20.0	987.4

Table 2 Designations, thermal properties of UHMWPE, UHMWPE/ANC, UHMWPE/ATANC and UHMWPE/FANC^{mx} as-prepared fibers and the corresponding compositions of gel solutions.

As-prepared fiber specimens	Weight or part of UHMWPE in gel solutions (g/phr)	Weight or part of ATANC in gel solutions (g/phr)	Weight or part of FANC^{mx} in gel solutions (g/phr)	Volumes of decalin in gel solutions (ml)	T_m (℃)	l_c (nm)	X_c (%)
F_{100}	2/100	-	-	100	142.7	31.9	65.1
$F_{100}ATANC_{0.025}$	2/100	0.0005/0.025	-	100	139.1	14.0	67.6
$F_{100}ATANC_{0.05}$	2/100	0.001/0.05	-	100	138.6	13.0	69.7
$F_{100}ATANC_{0.075}$	2/100	0.0015/0.075	-	100	138.2	12.2	71.3
$F_{100}ATANC_{0.1}$	2/100	0.002/0.1	-	100	137.6	11.3	72.1
$F_{100}ATANC_{0.125}$	2/100	0.0025/0.125	-	100	138.7	13.1	70.4
$F_{100}FANC^{m5}_{0.025}$	2/100	-	0.0005/0.025	100	138.7	13.1	69.3
$F_{100}FANC^{m5}_{0.05}$	2/100	-	0.001/0.05	100	138.3	12.4	69.8
$F_{100}FANC^{m5}_{0.075}$	2/100	-	0.0015/0.075	100	137.7	11.5	72.6
$F_{100}FANC^{m5}_{0.1}$	2/100	-	0.002/0.1	100	137.9	11.8	72.3
$F_{100}FANC^{m5}_{0.125}$	2/100	-	0.0025/0.125	100	138.2	12.2	71.8
$F_{100}FANC^{m10}_{0.025}$	2/100	-	0.0005/0.025	100	137.5	11.2	69.7
$F_{100}FANC^{m10}_{0.05}$	2/100	-	0.001/0.05	100	137.1	10.6	71.8
$F_{100}FANC^{m10}_{0.075}$	2/100	-	0.0015/0.075	100	136.8	10.3	73.6
$F_{100}FANC^{m10}_{0.1}$	2/100	-	0.002/0.1	100	136.9	10.4	72.9
$F_{100}FANC^{m10}_{0.125}$	2/100	-	0.0025/0.125	100	137.1	10.6	72.3
$F_{100}FANC^{m12.5}_{0.025}$	2/100	-	0.0005/0.025	100	136.6	10.0	69.8
$F_{100}FANC^{m12.5}_{0.05}$	2/100	-	0.001/0.05	100	136.4	9.8	72.7
$F_{100}FANC^{m12.5}_{0.075}$	2/100	-	0.0015/0.075	100	136.1	9.5	73.9
$F_{100}FANC^{m12.5}_{0.1}$	2/100	-	0.002/0.1	100	136.2	9.6	73.4
$F_{100}FANC^{m12.5}_{0.125}$	2/100	-	0.0025/0.125	100	136.2	9.6	72.5
$F_{100}FANC^{m15}_{0.025}$	2/100	-	0.0005/0.025	100	138.2	12.2	69.5
$F_{100}FANC^{m15}_{0.05}$	2/100	-	0.001/0.05	100	137.8	11.6	71.3
$F_{100}FANC^{m15}_{0.075}$	2/100	-	0.0015/0.075	100	137.4	11.0	72.8
$F_{100}FANC^{m415}_{0.1}$	2/100	-	0.002/0.1	100	137.6	11.3	72.5
$F_{100}FANC^{m415}_{0.125}$	2/100	-	0.0025/0.125	100	137.7	11.5	72.2
$F_{100}FANC^{m20}_{0.025}$	2/100	-	0.0005/0.025	100	138.9	13.5	69.1
$F_{100}FANC^{m20}_{0.05}$	2/100	-	0.001/0.05	100	138.4	12.6	70.6
$F_{100}FANC^{m20}_{0.075}$	2/100	-	0.0015/0.075	100	138.1	12.1	71.8
$F_{100}FANC^{m20}_{0.1}$	2/100	-	0.002/0.1	100	138.6	13.0	71.5
$F_{100}FANC^{m20}_{0.125}$	2/100	-	0.0025/0.125	100	138.7	13.1	71.3

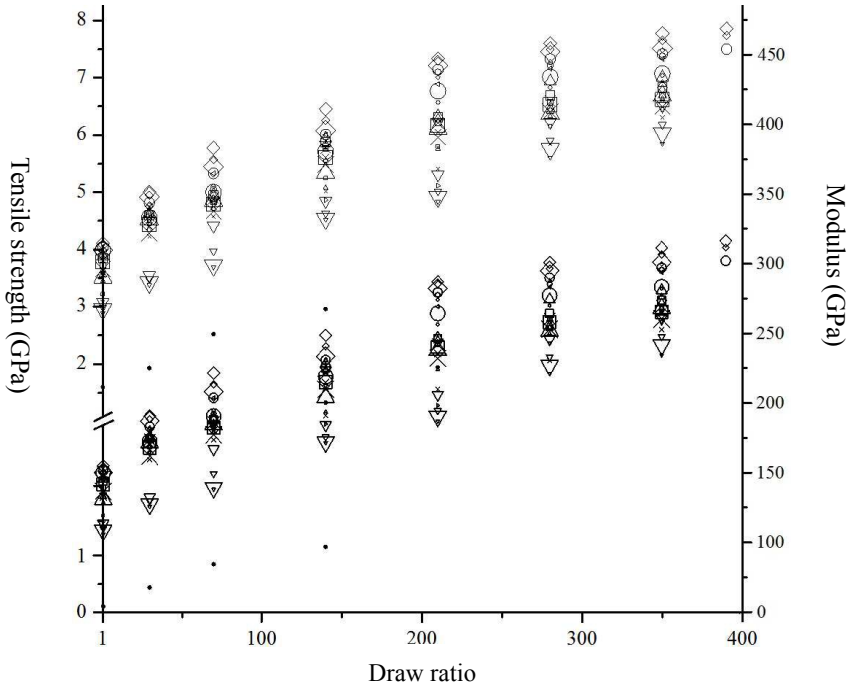

Tensile strength and modulus values of UHMWPE, UHMWPE/ANC, UHMWPE/ATANC and UHMWPE/FANC^{mx} fibers with varying draw ratios.